Coupled Lorenz oscillators near the Hopf boundary: Multistability, intermingled basins, and quasiriddling

Thierry T. Wontchui,[1,2] Joseph Y. Effa,[1] H. P. Ekobena Fouda,[3] Sangeeta R. Ujjwal,[4] and Ram Ramaswamy[2]

[1]*Department of Physics, Faculty of Science, The University of Ngaoundéré, P.O. Box 454 Ngaoundéré, Cameroon*

[2]*School of Physical Sciences, Jawaharlal Nehru University, New Delhi 110067, India*

[3]*Laboratoire d'Analyses, Simulations et Essais, IUT, The University of Ngaoundéré, Cameroon, P.O. Box 455 Ngaoundéré, Cameroon*

[4]*Department of Solar Energy and Environmental Physics, Blaustein Institutes for Desert Research, Ben-Gurion University of the Negev, Sede Boqer Campus, 84990, Israel*

(Received 19 September 2017; published 11 December 2017)

We investigate the dynamics of coupled identical chaotic Lorenz oscillators just above the subcritical Hopf bifurcation. In the absence of coupling, the motion is on a strange chaotic attractor and the fixed points of the system are all unstable. With the coupling, the unstable fixed points are converted into chaotic attractors, and the system can exhibit a multiplicity of coexisting attractors. Depending on the strength of the coupling, the motion of the individual oscillators can be synchronized (both in and out of phase) or desynchronized and in addition there can be mixed phases. We find that the basins have a complex structure: the state that is asymptotically reached shows extreme sensitivity to initial conditions. The basins of attraction of these different states are characterized using a variety of measures and depending on the strength of the coupling, they are intermingled or quasiriddled.

DOI: 10.1103/PhysRevE.96.062203

I. INTRODUCTION

For more than five decades now the Lorenz system [1]

$$\begin{aligned}\dot{x} &= \alpha(y - x)\\ \dot{y} &= \beta x - y - xz\\ \dot{z} &= -\gamma z + xy\end{aligned} \tag{1}$$

has been a very useful model on which many concepts and principles of nonlinear dynamical systems have been tested and illustrated. The parameters chosen in the initial study, namely $\alpha = 10$, $\beta = 28$, and $\gamma = 8/3$, have been most often used in numerical studies; these ensure a single chaotic attractor on which almost all the dynamics eventually settles, and it is easy to see that there are three other fixed points, all of which are unstable. Keeping α and γ at the same values, Sparrow [2] has given a fairly comprehensive description of the dynamical states when β is varied, and it is known that there are a number of other dynamical states and bifurcations that occur at different values of the parameters.

Within the phenomenon of chaos synchronization the Lorenz system has been extensively used as a paradigm, starting with the earliest studies [3,4] that introduced the notion of synchronization between coupled chaotic units. As is now well known, coupled chaotic systems can show a number of different forms of synchrony [4–8], depending on the nature of the coupling [9–11], its topology [10], as well as on the nature of the dynamical systems that are coupled [12]. Synchronization is attained between the systems when their trajectories (or states) get closer with the pairwise differences of the system variables approaching zero asymptotically. This phenomenon requires that the states of the system evolve in time, as when there are oscillations. Depending on the nature of the coupled systems and on the coupling scheme, different forms of synchronization can be observed [8,13]. There can be complete synchronization [10], the generalized synchronization [14], the phase synchronization [15], the anticipated synchronization [16], and so on. For the past few decades, interest in chaotic synchronization has grown considerably due to the potential applications it can have in diverse fields ranging from computational neuroscience [17] to secure communication [6,7,18].

In the present paper we revisit the dynamics of coupled Lorenz systems with parameters close to the subcritical Hopf bifurcation. For $\alpha = 10$ and $\gamma = 8/3$ for instance, this bifurcation occurs at $\beta = 24.74$, although there is already a strange attractor born at $\beta = 24.06$. This is the familiar butterfly-shaped attractor, at the "centers" of whose wings are unstable limit cycles that are created through a homoclinic bifurcation at $\beta = 13.926$. We examine the nature of the dynamics when the intrinsic parameters of the coupled systems are just above the Hopf bifurcation, and the nature of the dynamical phenomena induced by the coupling is qualitatively and quantitatively very different from the dynamics well above the bifurcation.

Our motivation arises in part from the observation [19] that coupling dynamical systems effectively alters the values of the parameters governing the flows. In addition the coupling can affect the stability of the coupled dynamics and therefore it becomes important to examine the dynamics of coupled systems in the neighbourhood of bifurcations since here fundamentally new phenomena can arise.

The present study is thus complementary to the work of Camargo, Viana, and Anteneodo [20] who examined the features of chaotic synchrony and antisynchrony [21] in coupled chaotic Lorenz oscillators. (Antisynchronization is characterized by the dynamical states of the subsystems having opposite signs.) Since both complete synchrony and antisynchrony coexist in the coupled system, the nature of the basins of the coexisting attractors has been described in great detail [20]. It has been established that for some range of the coupling strength the basins corresponding to

the coexisting attractors are both riddled and can therefore be termed intermingled. This intermingling structure of the basins is responsible of the complicated nature of the system making it unpredictable. However, this complexity and unpredictability is exacerbated further when the number and types of attractors increase.

We show here that for two mutually coupled identical Lorenz oscillators near the Hopf bifurcation point, depending upon the coupling strength there can be a large number of distinct dynamical states, leading to rich and complex dynamics in the system. The coexistence of a large number of attractors introduces additional sensitivity and randomness in the chaotic system: an infinitesimal perturbation in initial values is sufficient for a trajectory to shift from one state to another. This can be of great interest for applications in the field of secure communication through encryption of information based chaos for example. We describe and characterize the basins of attraction corresponding to different attractors using various measures such as transverse Lyapunov exponent, power-law relations, and so on. We observe that depending on the coupling value, the nature of the basins changes from quasiriddled to intermingled.

The remainder of the paper is organized as follows: Sec. II presents the model of mutually coupled Lorenz oscillators, and we describe the different attractors that are possible in the system. These are characterized using a modified version of the 0-1 test [22]. The basins of attraction of different states of the system are described in Sec. III. The fraction of initial conditions converging to these different states along with the extreme sensitivity to initial conditions is also quantified in this section. The riddled nature of the basins is discussed in Sec. IV and this is characterized using a variety of different quantitative measures. The paper concludes with a summary of our results in Sec. V.

II. COUPLED LORENZ SYSTEMS NEAR THE HOPF BIFURCATION

The Lorenz system, specified by Eq. (1) [1] has a number of interesting properties that include volume contraction, nonlinearity, and the discrete symmetry $(x,y) \to (-x,-y)$ [23]. In this paper we work at the "standard" values of $\alpha = 10$ and $\gamma = 8/3$. As described comprehensively by Sparrow [2], for $\beta \in$ [0-1[the fixed point (0, 0, 0) is stable. At $\beta = 1$, the origin loses stability in a supercritical pitchfork bifurcation and a pair of symmetric stable fixed points $C_+ = \sqrt{\beta(z-1)}$ and $C_- = -\sqrt{\beta(z-1)}$ appear. C_+ and C_- lose stability at $\beta_H = 24.74$ in a subcritical Hopf bifurcation by absorbing an unstable limit cycle [23]. For $\beta \in$ [13.926, 24.06[, there is transient chaos showing the presence of chaotic orbits but no chaotic attractors. For $\beta \in$ [24.06, 24.74], the two attracting equilibria C_+ and C_- coexist with the butterfly-shaped chaotic attractor. For $\beta > 24.74$, the dynamics of the system lies on the chaotic attractor and C_+ and C_- are unstable. These behaviors are illustrated in the bifurcation diagram in Fig. 1, obtained by plotting the successive maxima of the variable x.

The interest here is in the asymptotic dynamics of coupled Lorenz oscillators near the Hopf bifurcation transition, namely for $\beta = \beta_H + \delta$. Coupling two identical Lorenz systems mutually through the z variable so as to preserve the equivariance [2,24], one has the equations of motion:

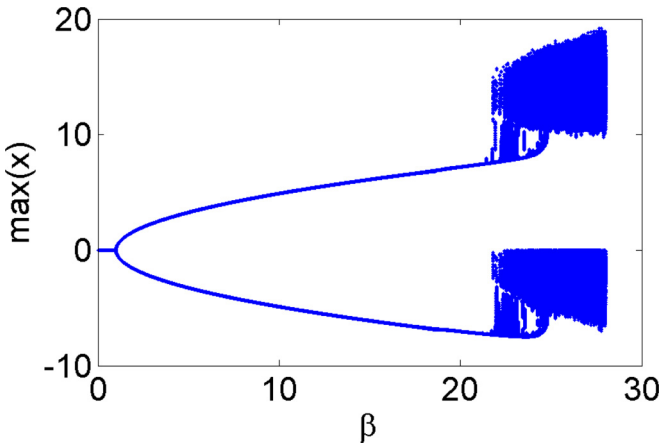

FIG. 1. Bifurcation diagram of the Lorenz system for $\alpha = 10$ and $\gamma = 8/3$.

$$\begin{aligned}
\dot{x_1} &= \alpha(y_1 - x_1) \quad \dot{y_1} = \beta x_1 - y_1 - x_1 z_1 \\
\dot{z_1} &= -\gamma z_1 + x_1 y_1 + \varepsilon(z_2 - z_1) \\
\dot{x_2} &= \alpha(y_2 - x_2) \quad \dot{y_2} = \beta x_2 - y_2 - x_2 z_2 \\
\dot{z_2} &= -\gamma z_2 + x_2 y_2 + \varepsilon(z_1 - z_2). \qquad (2)
\end{aligned}$$

It is convenient to make a transformation to the new coordinates [20],

$$x = \frac{x_2 - x_1}{2}, \quad y = \frac{y_2 - y_1}{2}, \quad z = \frac{z_2 - z_1}{2},$$
$$X = \frac{x_2 + x_1}{2}, \quad Y = \frac{y_2 + y_1}{2}, \quad Z = \frac{z_2 + z_1}{2},$$

which permits the coupled system to be rewritten as

$$\begin{aligned}
\dot{x} &= \alpha(y - x) \quad \dot{y} = \beta x - y - (Xz + Zx) \\
\dot{z} &= -(\gamma + 2\varepsilon)z + Xy + Yx \\
\dot{X} &= \alpha(Y - X) \quad \dot{Y} = \beta X - Y - (XZ + xz) \\
\dot{Z} &= -\gamma Z + XY + xy. \qquad (3)
\end{aligned}$$

Either Eq. (2) or Eq. (3) will be used below as convenient. Note that the dynamics of Eq. (3) is invariant under the transformations $(x,y,z) \to (-x,-y,-z)$. The condition $x_1 = x_2$, $y_1 = y_2$, $z_1 = z_2$ or equivalently $x = y = z = 0$ specifies a three-dimensional invariant subspace, the synchronization manifold, $\mathcal{S}_s$. The coupled system is also invariant under the transformations $(X,Y,z) \to (-X,-Y,-z)$ and the condition $X = Y = z = 0$, which corresponds to $x_1 = -x_2$, $y_1 = -y_2$, $z_1 = z_2$ defines the antisynchronization manifold $\mathcal{S}_{as}$ which is also an invariant subspace. Note that within $\mathcal{S}_s$ the equations of motion for the variables (X,Y,Z) have the same form as the Lorenz equations, Eq. (1): there is another attractor, denoted A_s contained in $\mathcal{S}_s$. The variables (x,y,Z) also obey Lorenz dynamics and give rise to the attractor A_{as}, which is contained in $\mathcal{S}_{as}$. We find that the *number* of attractors in these subspaces, namely A_s and A_{as}, depends on the coupling strength, and near the Hopf bifurcation point, this number changes.

Consider the case of weak coupling, namely ε small. Upon decreasing the parameter β from 28 (when the isolated systems

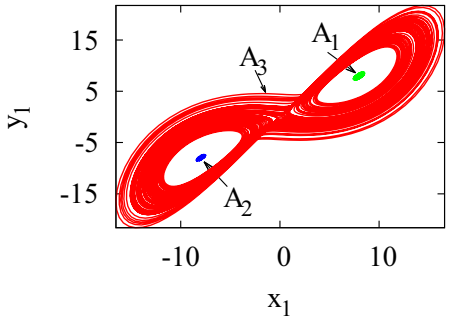

FIG. 2. The three types of attractors observed by coupling two Lorenz oscillators for the parameters $\beta = 24.76$ and $\varepsilon = 0.05$. A_1 and A_2 are the two small symmetric ones and A_3 the familiar chaotic Lorenz attractor with the butterfly shape.

support a single strange attractor that we term A_3) down to β_H at some point (depending on the value of coupling strength ε) there is a transition to a regime of β where two new symmetric stable attractors, A_1 and A_2 can be observed. An example of these three coexisting attractors can be seen in Fig. 2; our calculations are carried out for $\delta = 0.02$, namely $\beta = 24.76$ using a standard Runge-Kutta code and we have taken $\varepsilon = 0.05$. The initial conditions were chosen randomly [25] and expanded views of A_1 and A_2 are displayed (after discarding transients) in Fig. 3. It should be noted that these attractors are similar to those reported earlier by Ujjwal *et al.* [19], where chimera states in an ensemble of globally coupled Lorenz

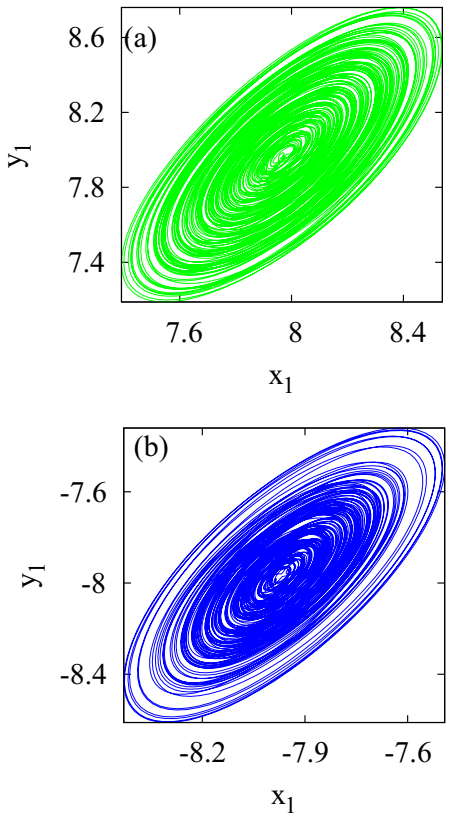

FIG. 3. Expanded view of attractor A_1 in (a), and its symmetric partner A_2 in (b).

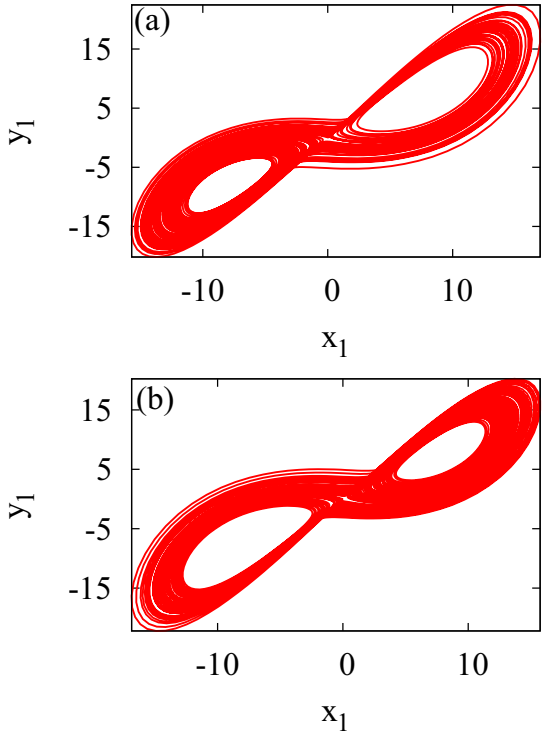

FIG. 4. The two different chaotic attractors with butterfly shape, (a) A_{3+} and (b) A_{3-}. The system parameters are $\beta = 24.76$ and $\varepsilon = 0.05$.

oscillators were studied. It was proposed that the attractors A_1 and A_2 appear as a result of change in the effective parameters of the system and the effective modulation of symmetric fixed points due to coupling between the oscillators.

Attractors A_1 and A_2 can easily be observed in the range $24.74 < \beta \lesssim 24.8$ with coupling strength $\varepsilon \in [0.05, 0.65]$. However, the probability of an initial condition to asymptotically reach these attractors (A_1 and A_2) is very low for $\beta \gtrsim 24.8$ and seems essentially to be null above $\beta \approx 26$. The relative sizes of the attractors A_1 and A_2 as well as the relative volumes of their basins decrease as β moves away from the subcritical Hopf bifurcation, making them difficult to observe.

The more familiar chaotic attractor A_3 has two variants, denoted $A_{3\pm}$. The distinction between these is that the scrolls are asymmetrical: A_{3-} and A_{3+} are plotted for $\beta = 24.76$ and $\varepsilon = 0.05$ in Fig. 4. The attractors A_{3+} and A_{3-} can be distinguished by computing the means M defined as follows:

$$M = \frac{x_{\max} + x_{\min}}{2}, \tag{4}$$

where $x_{\max}$ and $x_{\min}$ represent the maximum and minimum of the x variable after the transients. M is negative for A_{3-} and positive for A_{3+}.

To investigate the nature of attractors A_1 and A_2, we analyze the time series data corresponding to these attractors by means of a modification of the 0-1 test for the detection of chaos [26]. Note that A_1 and A_2 are generated by a suboscillator of the coupled system. Therefore, we find this technique more suitable for the analysis than the traditional method such as

computation of Lyapunov exponents, in the sense that the time series of the suboscillator can directly be applied to the test. Recall that the 0-1 test [22,27] is a binary chaos detection tool, which takes as input the time series data generated by a given deterministic dynamical system and returns a single value 0 or 1 according to whether the dynamics of the system is regular or chaotic. To use this technique, one neither requires to know the equations governing the system nor phase space reconstruction. The implementation of the test does not depend on the nature of the vector field as well as its dimensionality. The 0-1 test has been successfully applied to numerical [28] as well as experimental data [29], and its reliability has been established [30]. Implementation of this test is as follows [27]. Given an observable $\phi(j)$ with $j = 1,2,\ldots,N$, we first determine the translation variables $p(n)$ and $q(n)$ of $\phi(j)$:

$$p(n) = \sum_{j=1}^{n} \phi(j)\cos(jc),$$
$$q(n) = \sum_{j=1}^{n} \phi(j)\sin(jc), \tag{5}$$

where $c \in (0,\pi)$ and $n = 1,2,\ldots,N$. If the plot of $p(n)$ versus $q(n)$ is a torus the dynamics is regular, whereas if it behaves like a Brownian motion, the dynamics is chaotic. The behavior of $p(n)$ and $q(n)$ is investigated by computing the mean-square displacement (MSD) $D(n)$,

$$D(n) = \lim_{N\to\infty} \frac{1}{N}\sum_{j=1}^{N}\{[p(j+n)-p(j)]^2 + [q(j+n)-q(j)]^2\} - (E_\phi)^2\frac{1-\cos nc}{1-\cos c}, \tag{6}$$

with $n = 1,2,\ldots,N/10$ and $E_\phi = \lim_{N\to\infty}\frac{1}{N}\sum_{j=1}^{N}\phi(j)$ being the time average of the time series. When the MSD versus n is bounded in time, the dynamics of the system is regular, whereas if it scales linearly with time, the dynamics is chaotic. The asymptotic growth rate K_c of the MSD, representing the output of the test, is computed

$$K_c = \frac{\mathrm{cov}(\xi,\Delta)}{\sqrt{\mathrm{var}(\xi)\mathrm{var}(\Delta)}}, \tag{7}$$

where $\xi = 1,2,\ldots,N/10$ and $\Delta = D(1),D(2),\ldots,D(N/10)$ are two vectors. For some isolated values of c the test can give erroneous results due to resonances. To avoid this problem we have found it useful to compute the asymptotic growth rate for several values of c (typically 100 are sufficient to obtain reliable results), and the final K is obtained by computing the median of these isolated K_c's: $K \approx 0$ signifies regular dynamics and $K \approx 1$ implies chaos.

Nevertheless, for accurate results the 0-1 test requires a huge amount of data and is computationally expensive. Further, the test is unreliable when the time series are oversampled, and to overcome some of these limitations, we have, in earlier work, modified it as follows [26]: we analyze only the extrema rather than the time series itself and have obtained good results [31]. This modified test is applied to the analysis of the dynamics on the attractors A_1 and A_2, and the results are given in Fig. 5.

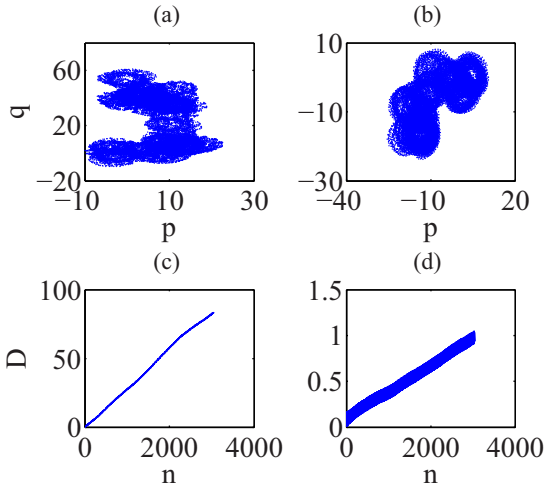

FIG. 5. Analysis of the dynamics of A_1 and A_2 by means of the modified 0-1 test. (a) and (b) are the translation variables p versus q of A_1 and A_2, respectively. (c) and (d) represent their MSD.

Figures 5(a) and 5(b) show the translation variables p versus q of A_1 and A_2, respectively. They behave like a Brownian motion which suggests that both A_1 and A_2 have chaotic dynamics. The motions of p and q are investigated by computing the MSD D that scales linearly with n for both A_1 Fig. 5(c) and A_2 Fig. 5(d), indicating that the attractors are chaotic. Finally, the asymptotic growth rate K of MSD has been computed. K is almost 1 for both cases, thus supporting the chaotic nature of A_1 and A_2.

The coupled Lorenz system for β just above the Hopf bifurcation shows very rich dynamics due to the existence of these several attractors: depending upon the initial conditions in the phase space and/or the coupling strength, the system can asymptote on a variety of different states. These can be confined within the synchronized or antisynchronized subspaces, or can be in the complement of these subspaces. A form of intermittency is also seen: trajectories are in the vicinity of $\mathcal{S}_s$ or $\mathcal{S}_{as}$ for varying periods of time, displaying intermittent synchronization or intermittent antisynchronization. Switching between these states is also possible. The taxonomy of the possible different states and their basins of attraction are discussed in the following section.

III. THE ATTRACTORS AND THEIR BASINS

The set of initial states that lead to a given attractor is its basin. While considering the situation where riddled basins can occur, for example, an attractor may be defined as follows [32]: Let $\mathcal{H}$ be the phase space in which the dynamical system $\mathcal{X}$ is defined. A closed subset $\mathcal{A} \in \mathcal{H}$ is an attractor of $\mathcal{X}$ if it satisfies the following conditions:

(i) $\mathcal{A}$ has a basin of attraction, denoted $\mathcal{B}(\mathcal{A})$, of positive Lebesgue measure (volume) in the phase space $\mathcal{H}$.

(ii) $\mathcal{A}$ is a compact set with a dense orbit. It should be noted that the basin of attraction does not need to include the whole neighborhood of the attractor.

When, as in the present instance, there is more than one attractor, then the geometries of the different basins become

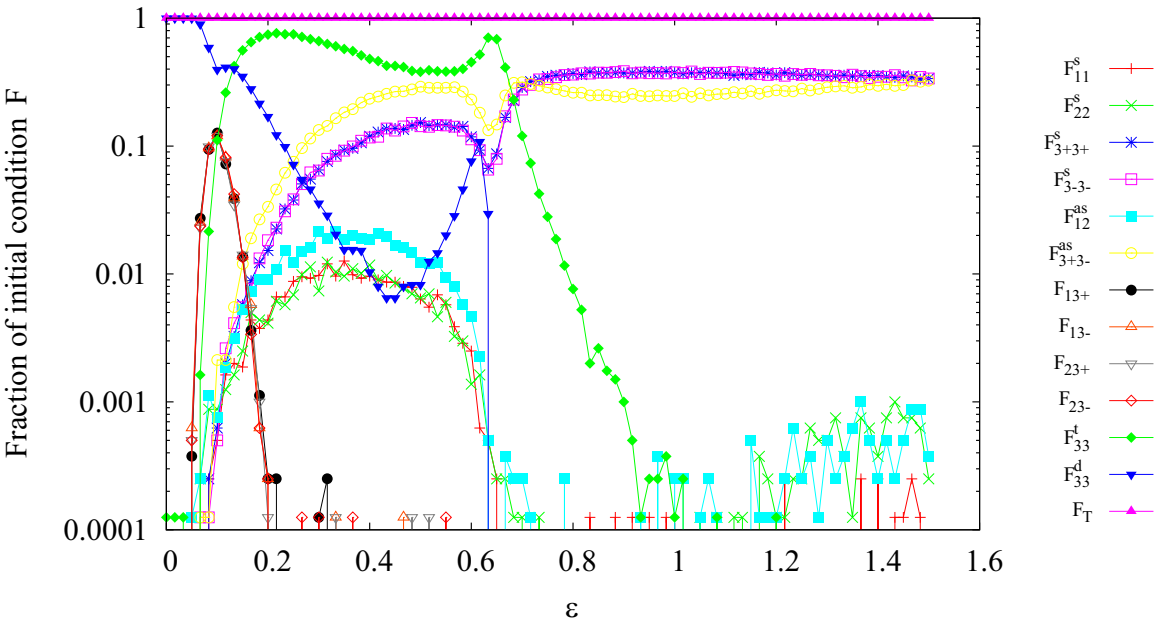

FIG. 6. Fraction of initial conditions F converging to the different attractors for the coupled Lorenz system as a function of ε for $\beta = 24.76$. Note that for $\varepsilon = 0$, namely for no coupling the only attractor of the dynamics is $\mathfrak{A}^d_{33}$, namely in each of the subsystems, the dynamics is independently on an attractor of type A_3.

a matter of considerable interest. As noted in the previous section, the phase space for the coupled Lorenz system is six-dimensional, and the spaces $\mathcal{S}_s$ and $\mathcal{S}_{as}$ have three dimensions.

Since the uncoupled oscillators are identical, and given the various symmetries in the phase space, we find that in the coupled system there is both complete synchronization when the two subsystems are identical, and antiphase synchronization like antisynchronization, when the dynamics differs by a phase. For the coupled system, according to the initial conditions and system parameters, attractors can be either in synchronization when both oscillators converge to either A_1 or A_2 or A_{3-} or A_{3+} so that the difference of their dynamical variables vanish in time, and these states are denoted by $\mathfrak{A}^s_{11}$,$\mathfrak{A}^s_{22}$,$\mathfrak{A}^s_{3-3-}$, and $\mathfrak{A}^s_{3+3+}$, respectively. It can also happen that the subsystem dynamics are in antisynchronization as when one oscillator asymptotes to A_1 and the other to A_2, or one oscillator asymptotes to A_{3+} and the other to A_{3-}. In this case, the sum of the dynamical variables vanish in time, and these states are therefore denoted $\mathfrak{A}^{as}_{12}$ and $\mathfrak{A}^{as}_{3+3-}$, respectively.

There can also be mixed phases, one oscillator converging to A_1 or A_2 and the other to A_{3+} or to A_{3-}. The notation we use is straightforward: $\mathfrak{A}_{13+}$, $\mathfrak{A}_{13-}$, $\mathfrak{A}_{23+}$ or $\mathfrak{A}_{23-}$, respectively; in the desynchronized configuration $\mathfrak{A}^d_{33}$, neither the difference nor the sum of the variables of the two subsystems vanish in time. The desynchronization can also be intermittent, but it is not clear whether this behavior is merely transient or not; there appears to be intermittent synchronization, intermittent antisynchronization, and a two-state intermittency as well, but these distinctions are more qualitative than quantitative. When constructing the basins of attraction of the system we only consider a single asynchronous state $\mathfrak{A}^d_{33}$.

The relative fraction of the phase space that leads to these different attractors changes with coupling strength, and the dependence is shown in Fig. 6 where the fraction of initial conditions converging to each attractor is plotted as a function of ε. The dependence is similar to that seen in some previous studies [21,33], which have noted that intermittent synchronization precedes complete synchronization. Here, however, we observe that intermittent synchronization and antisynchronization coexist with complete synchronization or antisynchronization over a substantial range of coupling parameter. The number of observable attractors depends on the strength of coupling as shown in Fig. 6. A sample of N randomly chosen initial conditions was evolved, and for each initial condition, we determine the state to which the system converges asymptotically from which the fraction of initial conditions going to each attractor, giving an estimate of the volume in phase space that the basin of the given attractor occupies.

In the absence of coupling only the desynchronized state $\mathfrak{A}^d_{33}$ exists with all initial conditions going to chaotic attractors of A_3 type in either oscillator. As ε increases, above a threshold $\varepsilon \approx 0.05$, attractors A_1 and A_2 emerge and consequently in the coupled system the synchronized states $\mathfrak{A}^s_{11}$, $\mathfrak{A}^s_{22}$, $\mathfrak{A}^s_{3+3+}$, and $\mathfrak{A}^s_{3-3-}$ can be seen in proportion to the fractions F^s_{11}, F^s_{22}, F^s_{3+3+}, F^s_{3-3-}, respectively. The antisynchronized attractors $\mathfrak{A}^{as}_{12}$, $\mathfrak{A}^{as}_{3+3-}$ have the fractions F^{as}_{12} and F^{as}_{3+3-} of initial conditions. It should be noted here that for symmetry reasons an equal number of initial conditions go to the attractors A_1 or A_2, and similarly to A_{3+} or A_{3-}. For the mixed phase states $\mathfrak{A}_{13+}$, $\mathfrak{A}_{13-}$, $\mathfrak{A}_{23+}$, $\mathfrak{A}_{23-}$ the corresponding fractions are denoted F_{13+}, F_{13-}, F_{23+}, and F_{23-}. All the intermittent synchronized attractors are clubbed together into F^t_{33}. Due to the emergence of these new attractors, the fraction of initial conditions going to the desynchronized attractor, F^d_{33} decreases with coupling strength. In the coupling range $0.1 \lesssim \varepsilon \lesssim 0.18$, the coupled system can exhibit as many as 14

TABLE I. Summary of the possible attractors in the coupled system depending on the strength of coupling ε for $\beta = 24.76$.

Coupling strength ε	$\varepsilon < 0.05$	$0.1 \lesssim \varepsilon \lesssim 0.18$			$0.18 \lesssim \varepsilon \lesssim 0.63$			$0.63 \lesssim \varepsilon \lesssim 1$		$1 \lesssim \varepsilon \lesssim 1.5$	
Possible attractors	$\mathfrak{A}^d_{33}$	$\mathfrak{A}^d_{33}$, $\mathfrak{A}^s_{3+3+}$, $\mathfrak{A}^{as}_{12}$, $\mathfrak{A}_{13+}$, $\mathfrak{A}_{23+}$,	$\mathfrak{A}^s_{11}$, $\mathfrak{A}_{23-}$,	$\mathfrak{A}^s_{22}$, $\mathfrak{A}^s_{3-3-}$, $\mathfrak{A}^{as}_{3+3-}$, $\mathfrak{A}_{13-}$, $\mathfrak{A}^t_{33}$	$\mathfrak{A}^d_{33}$, $\mathfrak{A}^s_{3+3+}$, $\mathfrak{A}^{as}_{12}$,	$\mathfrak{A}^s_{11}$, $\mathfrak{A}^{as}_{3+3-}$,	$\mathfrak{A}^s_{22}$, $\mathfrak{A}^s_{3-3-}$, $\mathfrak{A}^t_{33}$	$\mathfrak{A}^s_{3+3+}$, $\mathfrak{A}^{as}_{3+3-}$,	$\mathfrak{A}^s_{3-3-}$, $\mathfrak{A}^t_{33}$	$\mathfrak{A}^s_{3+3+}$, $\mathfrak{A}^{as}_{3+3-}$	$\mathfrak{A}^s_{3-3-}$, (mainly)

distinct states. When $\varepsilon \gtrsim 0.18$ the four mixed states vanish while the fraction of the synchronized, antisynchronized, and intermittent attractors increases. F^s_{11}, F^s_{22}, F^{as}_{12} reach their peak at $\varepsilon \approx 0.3$ and decrease with further increases in coupling strength. Finally, these states vanish along with F^d_{33} at $\varepsilon \approx 0.63$, where attractors $\mathfrak{A}^s_{3+3+}$, $\mathfrak{A}^s_{3-3-}$, $\mathfrak{A}^{as}_{3+3-}$ dominate, and their corresponding fractions continue to increase till they saturate at $\varepsilon \approx 0.8$. On the other hand, the intermittent attractors peak at $\varepsilon \approx 0.63$ and then decrease, vanishing at $\varepsilon \approx 1$. As can be seen in Fig. 6, for every ε, the sum of all fractions corresponding to each attractor, $F_T \approx 1$ indicating that there is substantially no other attractor in the system. The possible attractors for different coupling strength have been summarized in Table I.

To visualize the basin of an attractor, namely the set of initial conditions from which the trajectories start and then settle onto it after a long period of time [34], it is easier to display projections or phase space sections since the coupled system is six-dimensional. We constructed the sections by fixing the initial variables of the system as $x_1 = y_1 = x_2 = y_2 = 1$, and z_1, z_2 were selected randomly in the interval (20, 24). For each initial condition, the coupled system, Eq. (2) was evolved for sufficiently long times using a fourth-order Runge-Kutta algorithm, and then the final attractor was determined. Shown in Fig. 7 is this representative slice of the phase space indicating the initial conditions that result in $\mathfrak{A}^s_{11}$ (colored red), $\mathfrak{A}^s_{22}$ (green), $\mathfrak{A}^{as}_{12}$ (maroon), $\mathfrak{A}^s_{3+3+}$ (magenta), $\mathfrak{A}^s_{3-3-}$(white), $\mathfrak{A}^{as}_{3+3-}$ (black), $\mathfrak{A}^d_{33}$ (blue), $\mathfrak{A}_{13+}$ (yellow), $\mathfrak{A}_{13-}$ (orange), $\mathfrak{A}_{23+}$ (gray), and $\mathfrak{A}_{23-}$(chartreuse) for β=24.76.

Figure 7(a) displays the basin for a coupling strength $\varepsilon = 0.04$. For this coupling strength all initial conditions in the coupled system lead to the asynchronous attractor $\mathfrak{A}^d_{33}$. With increasing coupling strength, say $\varepsilon \approx 0.06$, intermittent behavior results: see Fig. 6. For higher coupling strength $\varepsilon = 0.1$ the several attractors described above are visible [see Fig. 7(b)] and upon further increasing the coupling to $\varepsilon = 0.35$, the mixed states disappear and fewer attractors become visible as can be seen in Fig. 7(c). When $\varepsilon = 0.7$ as in Fig. 7(d), the

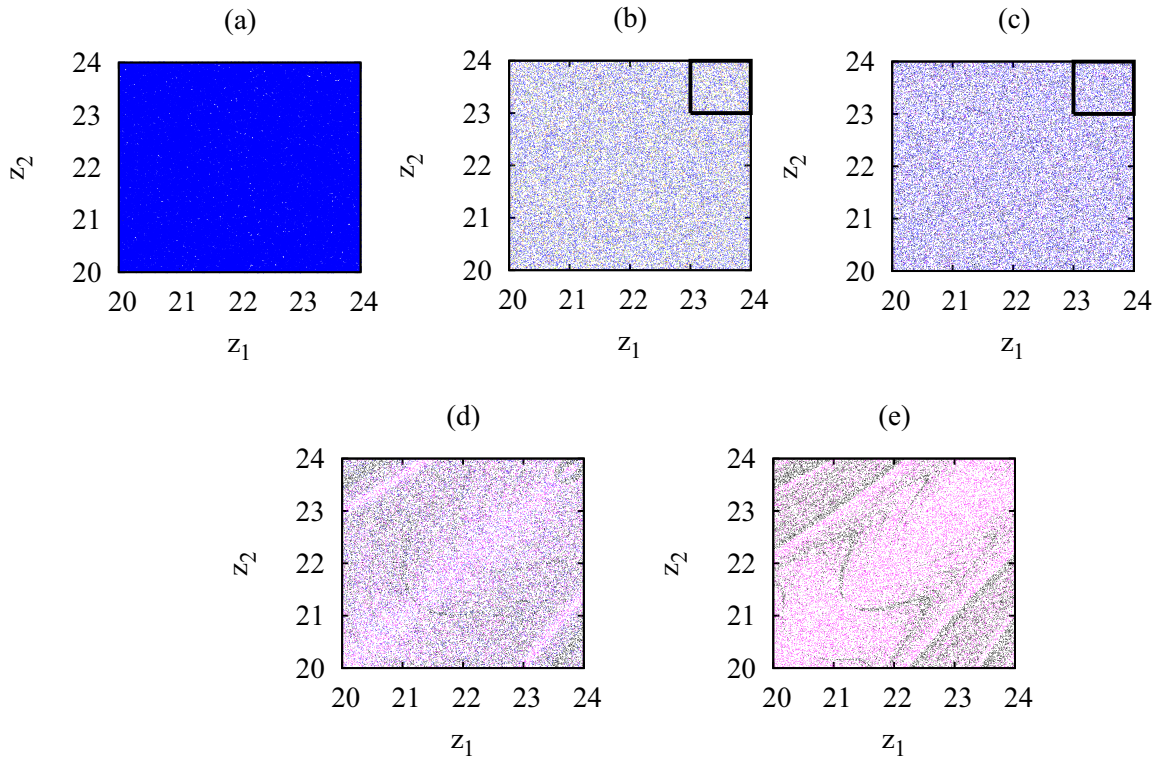

FIG. 7. Sections of the basins of attraction of the various attractors for the coupled Lorenz system when $\beta = 24.76$ with the coupling strength (a) $\varepsilon = 0.04$, (b) $\varepsilon = 0.1$, (c) $\varepsilon = 0.35$, (d) $\varepsilon = 0.7$, and (e) $\varepsilon = 1.1$. The initial conditions are chosen as described in the text and are colored according to which attractor they lead to as also described in the text. As can be seen, the number of attractors that are effectively visible depends on the coupling, and for sufficiently large ε, the basins are strongly intertwined.

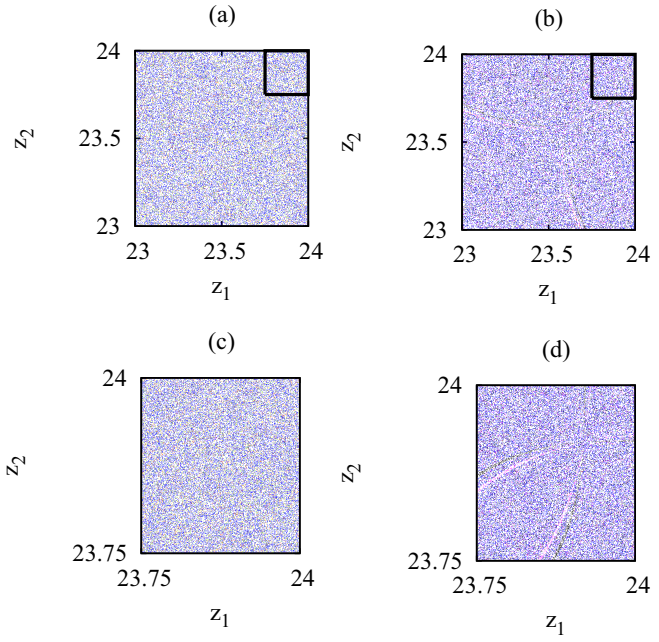

FIG. 8. Panels (a) and (b) are magnifications of the boxes in Figs. 7(b) and 7(c), respectively, while (c) and (d) are magnifications of square boxes in (a) and (b), respectively.

basins show the coexistence of four states namely the basins of $\mathfrak{A}^{s}_{3+3+}$, $\mathfrak{A}^{s}_{3-3-}$, $\mathfrak{A}^{as}_{3+3-}$, and $\mathfrak{A}^{d}_{33}$. Figure 7(e) shows the basins when $\varepsilon = 1.1$ when $\mathfrak{A}^{d}_{33}$ has disappeared and the basins of the three attractors $\mathfrak{A}^{s}_{3+3+}$, $\mathfrak{A}^{s}_{3-3-}$, and $\mathfrak{A}^{as}_{3+3-}$ are the only ones evident. This behavior is fairly typical even for somewhat higher values of β near the Hopf bifurcation point, say for $\beta = 24.78$, for example. In the regime of multistability [35], as can be seen in Fig. 7 the basins of the different attractors are highly intermixed and in the neighborhood of every initial condition leading to a particular attractor there are initial conditions arbitrarily nearby that asymptote to different attractors.

In fact, for dynamical systems with multiple attractors, the corresponding basins of attraction can exhibit a complicated structure with fractal basin boundary [36–38] or even more complex, with the so-called Wada property [39]. Accordingly, for a randomly chosen initial condition it is difficult to identify which attractor corresponds to it with certainty. The present example of coexisting attractors do appear to have basins with fractal boundaries. Repeated magnifications of regions in the phase space Figs. 7(b) and 7(c) show that the structures have increasingly finer detail as can be seen in Figs. 8(a) and 8(b) and further in Figs. 8(c) and 8(d). These magnifications reveal the self-similar structure, namely scale invariance, and it may therefore be anticipated that the present system will display final state sensitivity on initial conditions.

Final state sensitivity can be quantified through the uncertainty fraction [36,37], a measure that was proposed to evaluate the fractal nature of the basin in a given multistable dynamical system. This quantity can be determined as follows: an initial condition ic_1 is randomly selected in the phase space, here with coordinates (z_1, z_2) keeping $x_1 = y_1 = x_2 = y_2 = 1$. A second initial condition is also chosen at random, ic_2, a distance ξ from ic_1. The uncertainty fraction ρ is the probability that the

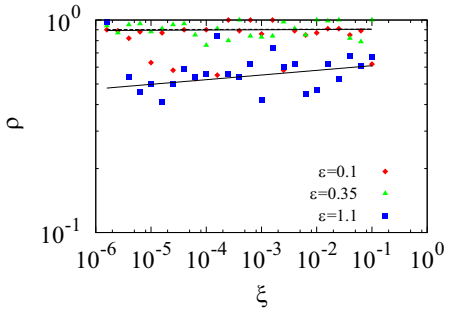

FIG. 9. Fraction of pairs of initial conditions going to different attractors, ρ where the initial conditions in each pair are ξ distance apart, shown for three different values of coupling strength ε. Linear fitting to the data (solid and dashed lines) gives uncertainty exponent, α. For $\varepsilon = 0.1$ the slope is $\alpha \approx 0.001 \pm 0.003$, for $\varepsilon = 0.35$, $\alpha \approx 0.0003 \pm 0.0005$, and for $\varepsilon = 1.1$,$\alpha \approx 0.02 \pm 0.008$.

two points ic_1 and ic_2 belong to basins of different attractors, namely this is essentially the probability to make an error while predicting the final state for a given initial condition. The measure ρ is expected to scale with the uncertainty radius ξ as $\rho \sim \xi^{\alpha}$, where $\alpha \geqslant 0$ is the uncertainty exponent that quantifies the degree of uncertainty in predicting the asymptotic state of the system for given initial condition.

In the case that α is zero or nearly zero, it is clear that there will be little improvement in the ability to find the correct asymptotic attractor with reducing the uncertainty ξ: this will not substantially decrease the uncertainty fraction ρ. For such an exponent, the asymptotic attractors are said to exhibit an extreme type of sensitive dependence on initial conditions [40], which makes the system utterly unpredictable. Shown in Fig. 9 are results of the above procedure to determine ρ as a function of ξ for different values of the coupling.

As may be inferred from Fig. 9, the uncertainty exponents are all nearly zero, which indicate the extreme type of sensitive dependence of the asymptotic attractors on initial conditions. Moreover, the uncertainty dimension d of the fractal basin boundary should be close to the phase space dimension D, which is related to the uncertainty exponent as $\alpha = D - d$ [37]. As for all cases $\alpha \approx 0$, thus $d \approx D$, supporting the extreme type of sensitivity of the coexisting attractors. Therefore, the coupled system for given parameters exhibits very complicated dynamics in terms of the predictability of asymptotic attractors for specified initial values. This predictability is in a sense harder than the case exhibited by systems with ordinary fractal or Wada properties. However, such an extreme type of sensitivity of asymptotic attractors on initial conditions are characteristic of riddling phenomenon or riddling-like structure.

IV. RIDDLING BEHAVIOR IN BASINS OF ATTRACTION

For a dynamical system with multiple attractors, the concept of riddling was first introduced and studied in Ref. [41] for the situation where the basin of a chaotic attractor in a symmetric invariant subspace is punctured with holes containing initial conditions belonging to the basin of another attractor (whether chaotic or not). Moreover, this first chaotic attractor should be stable with respect to transverse perturbations, namely the

transverse Lyapunov exponent should be negative [40–42]. However, when in the same system more than one attractor is riddled, the basin structure is said to be intermingled [41]. Attractors in this context must be considered in the sense of Milnor [32]: any starting point in the neighborhood of one attractor can converge onto another attractor. It has been established that riddling occurs when the low period unstable periodic orbits embedded within the chaotic attractor become transversely unstable [43]. This can also be induced through small amplitude random noise [44], and depending on the manner in which these orbits lose stability, different types of riddling bifurcations have been reported [42,43,45].

We briefly recall the conditions that need to be satisfied to classify attractor basins as being riddled [38,41,42]:

(i) There is an invariant subspace of dimension lower than that of the phase space of the system and which contains a chaotic attractor.

(ii) There is another attractor (chaotic or not) outside this invariant subspace.

(iii) The chaotic attractor is transversely stable in the phase space. The Lyapunov exponents transverse to the invariant subspace, $\lambda_\perp$, are negative.

(iv) A set of unstable periodic orbits embedded in the chaotic attractor are transversely unstable, and therefore for at least one of the negative transverse Lyapunov exponents, there should be substantial positive finite-time fluctuations.

As discussed above in Sec. II the present system of coupled Lorenz oscillators has two distinct three-dimensional subspaces $\mathcal{S}_s$ and $\mathcal{S}_{as}$. The emergence of four different attractors for each subsystem denoted A_1, A_2, A_{3+}, and A_{3-}, leads the coupled system to six different invariant subspaces namely $\mathcal{S}_{1s}$, $\mathcal{S}_{2s}$, $\mathcal{S}_{3+s}$, $\mathcal{S}_{3-s}$ within the synchronization manifold, and $\mathcal{S}_{12as}$, $\mathcal{S}_{3+3-as}$ on the antisynchronization manifold. For complete synchronization and antisynchronization, these subspaces are invariant since trajectories starting there will remain there. Moreover, in the synchronization manifolds $\mathcal{S}_{1s}$, $\mathcal{S}_{2s}$, $\mathcal{S}_{3+s}$, $\mathcal{S}_{3-s}$ contain, respectively, the chaotic attractors $\mathfrak{A}^s_{11}$, $\mathfrak{A}^s_{22}$, $\mathfrak{A}^s_{3+3+}$, and $\mathfrak{A}^s_{3-3-}$. Similarly, in the antisynchronization manifolds $\mathcal{S}_{12as}$ and $\mathcal{S}_{3+3-as}$ contain the chaotic attractors $\mathfrak{A}^{as}_{12}$ and $\mathfrak{A}^{as}_{3+3-}$, respectively. Thus, conditions (i) and (ii) are fulfilled. It should be noted here that the mixed-phase and asynchronous attractors do not lie in invariant subspaces, and therefore their basins cannot be riddled. To verify condition (iii) we computed the largest Lyapunov exponent transverse to the synchronized invariant subspaces $\lambda_\perp$ using the variational equations for (x,y,z) [Eq. (8)] given below, setting $x = y = z = 0$:

$$\begin{aligned}
\dot{\delta x} &= \alpha(\delta y - \delta x)\\
\dot{\delta y} &= \beta\delta x - \delta y - X\delta z - Z\delta x\\
\dot{\delta z} &= -(\gamma + 2\varepsilon)\delta z + X\delta y + Y\delta x\\
\dot{X} &= \alpha(Y - X)\\
\dot{Y} &= \beta X - Y - XZ\\
\dot{Z} &= -\gamma Z + XY. \qquad (8)
\end{aligned}$$

We integrate the system with initial conditions $\delta x = \delta y = \delta z = 0$, $X = Y = 1$, and Z chosen randomly in the interval [20,24]. We also determine the three largest Lyapunov exponents of the coupled system [Eq. (2)] using the algorithm of Wolf and coworkers [46]. The attractors are chaotic, and the red, green, and blue curves shown in Fig. 10 represent the three largest Lyapunov exponents as a function of ε.

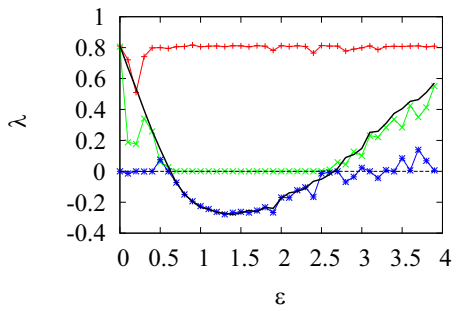

FIG. 10. The three largest Lyapunov exponents (red, green, and blue) of the coupled system [Eq. (2)] as a function of coupling strength ε. The black curve is the largest transversal Lyapunov exponent.

The largest (red curve) is always positive, attesting to the chaotic dynamics on the attractors. The chaotic nature of the attractors is also supported by $K \approx 1$ obtained from the modified 0-1 test for all values of ε (the result not shown here). There is always a component formed by part of second and third exponents which are near zero and represents the displacement along the trajectory while the third exponent (blue stars) represents the largest transversal Lyapunov exponent. The black curve is the largest transversal Lyapunov exponent calculated from the variational equations [Eq. (8)]. Results from both methods show that the largest transversal Lyapunov exponent changes sign at $\varepsilon_1 \approx 0.63$, the riddling bifurcation point and $\varepsilon_2 \approx 2.6$, the blowout bifurcation point [42]. For $\varepsilon_1 \leqslant \varepsilon \leqslant \varepsilon_2$ the only coexisting chaotic attractors are $\mathfrak{A}^s_{3+3+}$ and $\mathfrak{A}^s_{3-3-}$ in the synchronization manifold, $\mathfrak{A}^{as}_{3+3-}$ in the antisynchronization manifold, and partially the asynchronous state $\mathfrak{A}^d_{33}$ that is formed by intermittent synchronization and antisynchronization; see Fig. 6. It should be noted that it is possible to also find attractors $\mathfrak{A}^s_{11}$, $\mathfrak{A}^s_{22}$, and $\mathfrak{A}^{as}_{12}$, but their fractions are inconsiderable. In this interval, the largest transverse Lyapunov exponent for chaotic attractors in the synchronization and antisynchronization manifolds overlap for both methods and are negative. Thus, condition (iii) is fulfilled when $\varepsilon_1 \leqslant \varepsilon \leqslant \varepsilon_2$.

Although the chaotic attractors $\mathfrak{A}^s_{3+3+}$, $\mathfrak{A}^s_{3-3-}$, and $\mathfrak{A}^{as}_{3+3-}$ are all transversely stable, they contain unstable periodic orbits embedded within that are transversely unstable: this is indicated by positive finite-time Lyapunov exponent values denoted by $\tilde{\lambda}_\perp$. These unstable segments of the orbits are responsible for the repulsion of trajectories in the vicinity of the attractor. We have computed finite-time contributions to the largest transversal Lyapunov exponent using Eq. (8). The probability distribution function of the finite-time Lyapunov exponents is plotted in Fig. 11 for time $t = 20$ and for different values of ε. As can be clearly seen, the distribution of finite-time Lyapunov exponents is Gaussian with negative mean but extends to positive values. Similar distributions can be obtained for other values of the finite-time interval, t.

The fraction of positive finite-time Lyapunov exponents can be estimated by evaluating the integral $\varphi(t) = \int_0^\infty P(\tilde{\lambda}_\perp(t))d\tilde{\lambda}_\perp(t) > 0$ [38]. This is shown in Fig. 12 for different t as a function of ε. For $\varepsilon < \varepsilon_1$, $\varphi \approx 1$ meaning

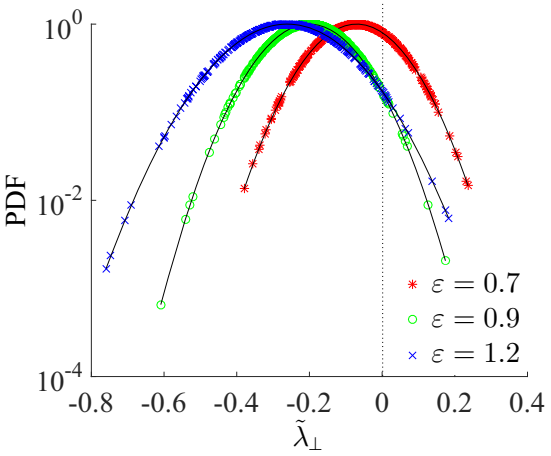

FIG. 11. Probability distribution function PDF of finite $t = 20$ largest transversal Lyapunov exponent for different values of ε.

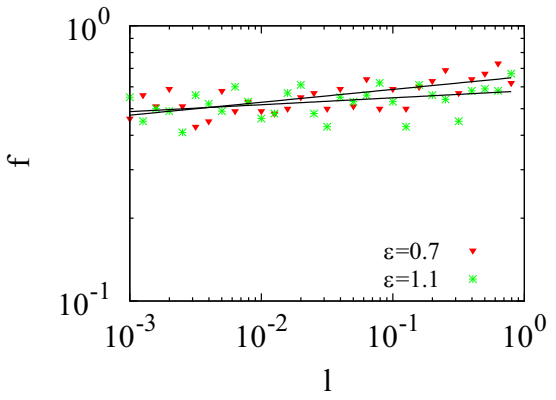

FIG. 13. Fraction of initial conditions f not converging to attractor $\mathfrak{A}^s_{3+3+}$ in the synchronized manifold $\mathcal{S}_{3+s}$ as a function of the distance l from the synchronized manifold $\mathcal{S}_{3+s}$ for different values of ε.

that the finite-time Lyapunov exponent is positive in average. This result agrees with the infinite-time transversal Lyapunov exponent (black curve), which is also positive as shown in Fig. 10. Then, φ decays to 0.5 at $\varepsilon = \varepsilon_1$ corresponding to the riddling bifurcation point for which $\lambda_\perp = 0$. Thereafter, φ drops below 0.5 for $\varepsilon > \varepsilon_1$. For this case, the finite-time transversal exponent is negative on average and agrees with Fig. 10. Hence, for $\varepsilon_1 < \varepsilon < \varepsilon_2$, φ is nonzero, although the largest transversal exponent is negative in average. The higher limit ε_2 defines the blowout bifurcation point through which the transversal exponent changes sign and becomes positive. However, for long time limit φ tends to be null, since the finite-time exponent is spread on a Dirac centered at $\lambda_\perp$ which is negative. Thus, condition (iv) for riddling basins is also fulfilled for this range of ε.

The riddling of the basins of attraction can also be investigated using scaling laws, namely, the measure of fraction of trajectories that asymptotes to a given attractor [42,47]. Consider the synchronization manifold $\mathcal{S}_{3+s}$ that contains the chaotic attractor $\mathfrak{A}^s_{3+3+}$. Attractor $\mathfrak{A}^s_{3+3+}$ is pierced by points containing initial conditions belonging to other attractors and any trajectory starting from these points will not converge to $\mathfrak{A}^s_{3+3+}$. Whenever $x = y = z = 0$, the system's trajectories will converge to either $\mathfrak{A}^s_{3+3+}$ or $\mathfrak{A}^s_{3-3-}$ of the synchronized manifolds depending on the initial condition.

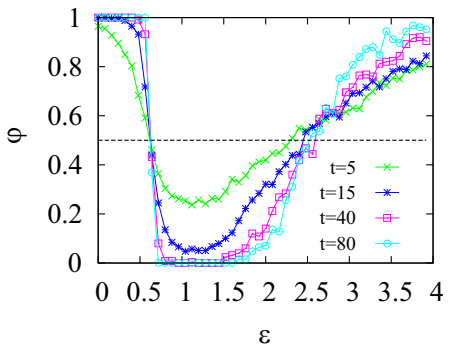

FIG. 12. Positive fraction φ of largest finite-time t transversal Lyapunov exponent as a function of ε, for different values of t interval.

The fraction $f_\star$ of points belonging to the basin of $\mathfrak{A}^s_{3+3+}$ in the synchronized manifold $\mathcal{S}_{3+s}$ is evaluated as follows: we first consider a set of initial conditions $x = y = z = 0$, $X = Y = 1$, and Z randomly chosen so that the system converges to attractor $\mathfrak{A}^s_{3+3+}$ in the invariant manifold $\mathcal{S}_{3+s}$. Then, for the same set of initial conditions but differing in the z direction by a distance $|z| = l$ we determine to which attractor the orbit converges. For each l, we repeat this operation for several values of Z. The fraction $f_\star$ is obtained by dividing the number of initial conditions for which the trajectories synchronize in $\mathcal{S}_{3+s}$ by the total number of initial conditions evolved. The fraction of trajectories that do not synchronize in $\mathcal{S}_{3+s}$ is obviously $f = 1 - f_\star$. For riddled basins, f should scale as a power of l as $f \sim l^\eta$, with $\eta > 0$ being the scaling exponent. Figure 13 presents results for two values of ε belonging to $[\varepsilon_1, \varepsilon_2]$ and as can be seen f shows fairly good scaling as a power of l.

Furthermore, riddling behavior can be manifested by extreme final states sensitivity on initial conditions. To verify this, the fraction of uncertain initial conditions going to different attractors, ρ as a function of distance between them can be plotted. For riddled basins, the uncertainty exponent should be close to zero, i.e., there is no change in the uncertainty fraction by decreasing the uncertainty level. Figure 9 shows the uncertainty fraction ρ for $\varepsilon = 1.1$ belonging to the riddling interval $[\varepsilon_1, \varepsilon_2]$. The uncertainty exponent was evaluated to be nearly zero ($\alpha \approx 0.02 \pm 0.008$).

Although $\varepsilon < \varepsilon_1$ is inside the multistability range, condition (iii) for riddled basins is not fulfilled due to the nonnegative transverse Lyapunov exponent. The coupled system exhibits an extreme type of sensitive dependence of asymptotic attractors on initial conditions as we showed in Sec. III, implying that a perturbation on initial conditions, no matter how small, has the same consequence as riddled basins regarding the ability to predict the final state of the system. The near-zero values of the uncertainty exponents indicate this and thus we term the resulting basins of attraction for this range of ε as "quasiriddled."

To summarize, for $\varepsilon_1 \leqslant \varepsilon \leqslant \varepsilon_2$ there are three chaotic attractors $\mathfrak{A}^s_{3+3+}$, $\mathfrak{A}^s_{3-3-}$, and $\mathfrak{A}^{as}_{3+3-}$ that occupy three-dimensional invariant subspaces, as well as the asynchronous

attractor $\mathfrak{A}_{33}^{d}$ that is in the six-dimensional phase space. The basin of each of the three attractors in the invariant subspace is riddled with holes containing initial conditions belonging to the basin of other coexisting attractors. Since more than one basin is riddled, the resulting coexisting basins are said to be intermingled. When $\varepsilon < \varepsilon_1$, the asymptotic attractors are extremely sensitive to initial conditions, thus sharing similarity with riddled basins in terms of predictability of the final states of the system, and hence can be termed quasiriddled.

V. CONCLUSION

In the present work we have studied the asymptotic behavior of a system of two mutually coupled identical Lorenz oscillators near the subcritical Hopf bifurcation point. Our motivation has been to explore the effect of coupling, namely the manner in which the coupling modifies the behavior.

Given the proximity of the bifurcation, the coupling results in the system displaying aspects of the dynamics of the uncoupled system below the bifurcation when there is multistability. In comparison with the studies that have examined coupled Lorenz systems for the "standard" parameter values, our work has uncovered a multiplicity of attractors that are not easily accessed far from the Hopf bifurcation. Indeed, the large number of attractors are uncharacteristic of coupled systems in which the dissipation is so large; instances of systems with a large number of coexisting attractors have frequently been observed for weakly dissipative dynamics. In this parameter regime, the system shows very rich dynamics. There are coexisting synchronized, antisynchronized, intermittent, mixed-phase, and desynchronized states, but depending on the coupling strength, different numbers of attractors are visible.

We have also examined the basins of attraction of these different states and found that the basins have a complicated structure that leads to unpredictable dynamics. Depending on the coupling strength value, the basins can be quasiriddled or intermingled. Such a coexistence of large number of attractors makes the chaotic coupled system highly sensitive to initial conditions, thus impeding our ability to predict the final state of the system. These properties can be of great significance in various areas of science and technology: multistability can be exploited in applications such as in the field of secure communication for instance. At the same time, it can also indicate features that need to be avoided to ensure stable dynamics.

Given such dynamical complexity in a system of two coupled Lorenz attractors, an ensemble of coupled Lorenz systems near the Hopf boundary—whether identical or not—will inevitably give rise to chimera states. Subsystem dynamics on the attractors of type A_1 or A_2 will almost surely be synchronized and antiphase to one another, while those subsystems that lead to the A_3 attractor will not be in synchrony. This mixture of synchrony and asynchrony can be seen to arise from the fact that there is multistability and that the basins of attraction have a complex intertwined structure.

We have not addressed the effect of noise which can play a major role when there are a large number of possible attractors. In particular, the intertwined nature of the basins of the different attractors makes the system extremely susceptible to fluctuations in the dynamics. These effects are being quantitatively studied in our ongoing work [48].

ACKNOWLEDGMENTS

T.T.W. was supported by the NAM S&T Centre (Centre for Science and Technology of the Non-Aligned and other Developing Countries), India under the Research Training Fellowship (RTF) for Developing Countries, 2016. S.R.U. acknowledges the support of the Jacob Blaustein Center for Scientific Cooperation, Israel through the award of a postdoctoral fellowship. R.R. is a recipient of the J. C. Bose National Fellowship of the SERB (Science and Engineering Research Board), Government of India, Grant No. DST-SR/S2/JCB/2008.

[1] E. N. Lorenz, J. Atmos. Sci. **20**, 130 (1963).
[2] C. Sparrow, *The Lorenz Equations: Bifurcations, Chaos, and Strange Attractors* (Springer, New York, 1982).
[3] H. Fujisaka and T. Yamada, Prog. Theor. Phys. **69**, 32 (1983).
[4] L. M. Pecora and T. L. Carroll, Phys. Rev. Lett. **64**, 821 (1990).
[5] S. Strogatz, *Synch: How Order Emerges from Chaos in the Universe, Nature, and Daily Life* (Hyperion, New York, 2003).
[6] L. Kocarev and U. Parlitz, Phys. Rev. Lett. **74**, 5028 (1995).
[7] L. M. Pecora, T. L. Carroll, G. A. Johnson, and D. J. Mar, Chaos **7**, 520 (1997).
[8] S. Boccaletti, J. Kurths, G. Osipov, D. L. Valladares, and C. S. Zhou, Phys. Rep. **366**, 1 (2002).
[9] Y. C. Lai and C. Grebogi, Phys. Rev. E **47**, 2357 (1993).
[10] R. Karnatak, R. Ramaswamy, and A. Prasad, Chaos **19**, 033143 (2009).
[11] K. Murali and M. Lakshmanan, Phys. Rev. E **49**, 4882 (1994).
[12] L. Huang, R. Feng, and M. Wang, Phys. Lett. A **320**, 271 (2004); S. Vaidyanathan, Int. J. Adv. Info. Tech. **1**, 13 (2011).
[13] A. Pikovsky, M. Rosenblum, and J. Kurths, *Synchronization: A Universal Concept in Nonlinear Sciences* (Cambridge University Press, Cambridge, 2001).
[14] H. D. I. Abarbanel, N. F. Rulkov, and M. M. Sushchik, Phys. Rev. E **53**, 4528 (1996).
[15] M. G. Rosenblum, A. S. Pikovsky, and J. Kurths, Phys. Rev. Lett. **76**, 1804 (1996).
[16] H. U. Voss, Phys. Rev. E **61**, 5115 (2000).
[17] F. Mormann, K. Lehnertz, P. David, and C. E. Elger, Phys. D **144**, 358 (2000).
[18] K. M. Cuomo and A. V. Oppenheim, Phys. Rev. Lett. **71**, 65 (1993).
[19] S. R. Ujjwal, N. Punetha, A. Prasad, and R. Ramaswamy, Phys. Rev. E **95**, 032203 (2017).
[20] S. Camargo, R. L. Viana, and C. Anteneodo, Phys. Rev. E **85**, 036207 (2012).
[21] C.-M. Kim, S. Rim, W.-H. Kye, J.-W. Ryu, and Y.-J. Park, Phys. Lett. A **320**, 39 (2003).
[22] G. A. Gottwald and I. Melbourne, Proc. Roy. Soc. A **460**, 603 (2004).

[23] S. H. Strogatz, *Nonlinear Dynamics and Chaos with Applications to Physics, Biology, Chemistry, and Engineering* (Perseus Books, New York, 1994).

[24] P. Chossat and R. Lauterbach, *Methods in Equivariant Bifurcations and Dynamical Systems* (World Scientific, Singapore, 2000).

[25] Initial conditions used to display the different attractors in Fig. 2 are given as: $(x_1,y_1,z_1) = (29.8273,12.9017,7.70745)$ and $(x_2,y_2,z_2) = (35.696,8.4582,11.8488)$ for A_1; $(x_1,y_1,z_1) = (43.7895,7.73186,17.9708)$ and $(x_2,y_2,z_2) = (32.7784, 28.9727,19.4601)$ for A_2; $(x_1,y_1,z_1) = (27.5994,21.2638, 37.1609)$ and $(x_2,y_2,z_2) = (14.5192,10.1428,33.3766)$ for A_3. Initial conditions used to plot A_{3-} and A_{3+} are given as: $(x_1,y_1,z_1) = (-45.63890,8.98617,37.8749)$ and $(x_2,y_2,z_2) = (-21.25766,6.10522,26.41834)$ for A_{3-}; $(x_1,y_1,z_1) = (-39.47111,13.13364,-16.02374)$ and $(x_2,y_2,z_2) = (35.25956,-9.26999,44.1614)$ for A_{3+}.

[26] J. S. A. E. Fouda, B. Bodo, S. L. Sabat, and J. Y. Effa, Int. J. Bifur. Chaos **24**, 1450063 (2014).

[27] G. A. Gottwald and I. Melbourne, SIAM J. Appl. Dyn. Syst. **8**, 129 (2008).

[28] G. Litak, A. Syta, and M. Wiercigroch, Chaos Solitons Fractals **40**, 2095 (2009); M. M. Aziz and M. N. Faraj, J. Emerg. Trends Comput. Inform. Sci. **3**, 783 (2012); C. Skokos, C. Antonopoulos, T. C. Bountis, and M. N. Vrahatis, J. Phys. A **37**, 6269 (2004).

[29] I. Falconer, G. A. Gottwald, I. Melbourne, and K. Wormnes, SIAM J. Appl. Dyn. Syst. **6**, 395 (2007).

[30] J. Hu, W. Tung, J. Gao, and Y. Cao, Phys. Rev. E **72**, 056207 (2005); G. A. Gottwald and I. Melbourne, *ibid.* **77**, 028201 (2008).

[31] T. T. Wontchui, J. Y. Effa, H. P. E. Fouda, and J. S. A. E. Fouda, Ann. Rev. Chaos Theor. Bif. Dyn. Syst. **7**, 1 (2017).

[32] J. Milnor, Comm. Math. Phys. **99**, 177 (1985).

[33] Y.-C. Lai and C. Grebogi, Phys. Rev. E **52**, R3313 (1995); L. Zhao, Y.-C. Lai, and C.-W. Shih, *ibid.* **72**, 036212 (2005).

[34] E. Ott, *Chaos in Dynamical Systems* (Cambridge University Press, Cambridge, 1993).

[35] A. N. Pisarchik and U. Feudel, Phys. Rep. **540**, 167 (2014).

[36] C. Grebogi, S. W. McDonald, E. Ott, and J. A. Yorke, Phys. Lett. A **99**, 415 (1983).

[37] S. W. McDonald, C. Grebogi, E. Ott, and J. A. Yorke, Physica D **17**, 125 (1985).

[38] J. Aguirre, R. L. Viana, and M. A. F. Sanjuan, Rev. Mod. Phys. **81**, 333 (2009).

[39] J. Kennedy and J. A. Yorke, Physica D **51**, 213 (1991); H. E. Nusse and J. A. Yorke, *ibid.* **90**, 242 (1996); J. Aguirre and M. A. F. Sanjuan, *ibid.* **171**, 41 (2002); Y. Zhang and L. F. Lu, Nonlinear Dyn. **77**, 1121 (2014).

[40] Y.-C. Lai, Phys. Rev. E **51**, 2902 (1995).

[41] J. C. Alexander, J. A. Yorke, Z. You, and I. Kan, Int. J. Bifur. Chaos **2**, 795 (1992).

[42] E. Ott, J. C. Alexander, I. Kan, J. C. Sommerer, and J. A. Yorke, Physica D **76**, 384 (1994).

[43] Y.-C. Lai, C. Grebogi, J. A. Yorke, and S. C. Venkataramani, Phys. Rev. Lett. **77**, 55 (1996).

[44] Y.-C. Lai and C. Grebogi, Phys. Rev. Lett. **77**, 5047 (1996).

[45] P. Ashwin, J. Buescu, and I. Stewart, Phys. Lett. A **193**, 126 (1994); Y. L. Maistrenko, V. L. Maistrenko, O. Popovych, and E. Mosekilde, Phys. Rev. E **60**, 2817 (1999).

[46] A. Wolf, J. B. Swift, H. L. Swinney, and J. A. Vastano, Physica D (Amsterdam) **16**, 285 (1985).

[47] E. Ott and J. C. Sommerer, Phys. Lett. A **188**, 39 (1994).

[48] T. T. Wontchui and R. Ramaswamy (unpublished).